J Comput Aided Mol Des (2014) 28:565–575
DOI 10.1007/s10822-014-9742-2

Theoretical studies on effective metal-to-ligand charge transfer characteristics of novel ruthenium dyes for dye sensitized solar cells

Huei-Tang Wang · Fadlilatul Taufany · Santhanamoorthi Nachimuthu · Jyh-Chiang Jiang

Received: 10 February 2014 / Accepted: 8 April 2014 / Published online: 18 April 2014

Abstract The development of ruthenium dye-sensitizers with highly effective metal-to-ligand charge transfer (MLCT) characteristics and narrowed transition energy gaps are essential for the new generation of dye-sensitized solar cells. Here, we designed a novel anchoring ligand by inserting the cyanovinyl-branches inside the anchoring ligands of selected highly efficient dye-sensitizers and studied their intrinsic optical properties using theoretical methods. Our calculated results show that the designed ruthenium dyes provide good performances as sensitizers compared to the selected efficient dyes, because of their red-shift in the UV–visible absorption spectra with an increase in the absorption intensity, smaller energy gaps and thereby enhancing MLCT transitions. We found that, the designed anchoring ligand acts as an efficient "electron-acceptor" which boosts electron-transfer from a –NCS ligand to this ligand via a Ru-bridge, thus providing a way to lower the transition energy gap and enhance the MLCT transitions.

Keywords Dye sensitized solar cells · Ruthenium complex · Absorption spectra · Density functional theory

Electronic supplementary material The online version of this article (doi:10.1007/s10822-014-9742-2) contains supplementary material, which is available to authorized users.

H.-T. Wang · F. Taufany · S. Nachimuthu (✉) · J.-C. Jiang (✉)
Department of Chemical Engineering, National Taiwan University of Science and Technology, Taipei 106, Taiwan, ROC
e-mail: santhanamoorthi@gmail.com

J.-C. Jiang
e-mail: jcjiang@mail.ntust.edu.tw

Introduction

Dye sensitized solar cells (DSSCs) are currently attracting widespread academic and industrial interest owing to their potential to harvest sunlight and convert it into electricity at low cost [1]. DSSCs formed as organometallic dyes adsorbed on nanocrystalline TiO_2 photoanodes have been intensively developed for the past two decades due to their high solar-to-electric conversion efficiency [2–4]. Among the various metal-transition based sensitizers, the Ru(II) based sensitizers are the most attractive due to their long-term stability, photophysical and electrochemical properties [5]. The first high-performance Ru(II)-sensitizer (termed as N3) was developed in 1993 by Nazeeruddin et al. [6] which consist of at least one 4,4′-dicarboxy-2,2′-bipyridine chelate (Fig. 1A) and reported overall power conversion efficiency of up to 10.0 %.

This N3 sensitizer is a naturally good visible-light absorber with a broad and strong visible absorption band dominated by the effective metal-to-ligand charge transfer (MLCT) transition [5–10]. For this effective MLCT transition, the electrons are promoted from the HOMO which is coming from the –NCS ligand, to the LUMO, in which these promoted electrons are ready to be injected into the semiconductor surface [11, 12]. However, this effective MLCT transition is not observed in the UV absorption region, thus there is difficulty in utilizing the UV absorption for electron-injection into a conduction band (CB) of semiconductor surface. Consequently, attempts have been made to improve the extent of effective MLCT transitions in particular visible regions gained huge significance for the development of DSSCs. It includes the design of Ru(II)-based sensitizers with amphiphilic properties and/or extended π-conjugation, to achieve a power conversion efficiency higher than that of N3. More specifically,

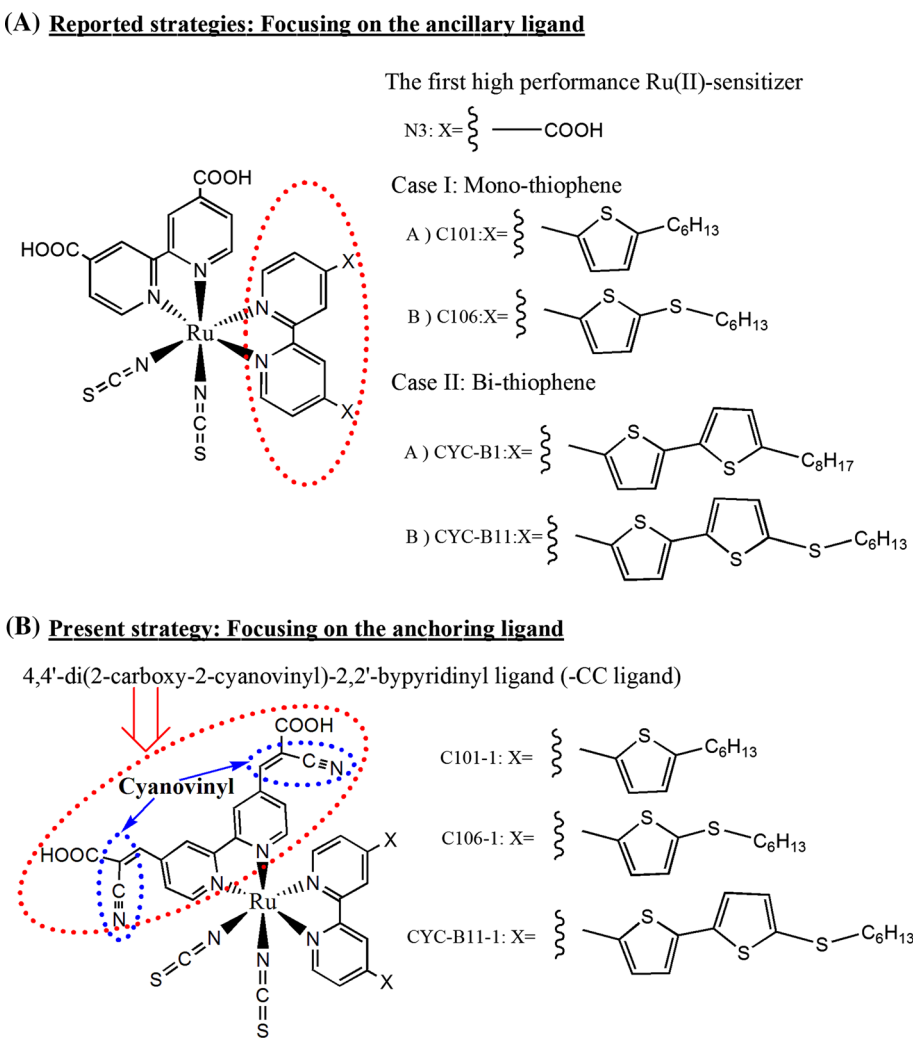

Fig. 1 Molecular structures of **A** the first high performance Ru(II) dye-sensitizer N3, and with those of heteroleptic ruthenium(II) dye-sensitizers C101, C106, CYC-B1, and CYC-B11, in comparison with their corresponding dye-sensitizer analogues: **B** C101-1, C106-1, and CYC-B11-1. These dye-sensitizer analogues were formed by modification on their anchoring ligands

Gao et al. [13] developed a Ru-sensitizer C101, in which one of the dicarboxylate-bypyridine ligands in N3 was replaced with a highly π-conjugated ancillary ligand i.e. alkyl-monothiophene (Fig. 1A-Case IA) and reached 11.3 % of power efficiency. Cao et al. [14] reported a C101 analogue (coded 106), with a sulfur atom inserted between the hexyl substituent and thiophene ring (Fig. 1A-Case IB) and found that the improved effective MLCT band light absorption coefficient (resulting power efficiency is about 11.4 %). In 2006, Chen et al. [7] reported the synthesis of Ru-sensitizer CYC-B1, by substituting the dicarboxylate-bypyridine ligands in N3 with highly conjugated alkyl-bithiophene ligands, as depicted in Fig. 1A-Case IIA. The resulting power conversion efficiency was found to be 10 % higher than that of N3 sensitizer. Following the development of the CYC-B1 sensitizer, a high absorption coefficient heteroleptic Ru-sensitizer, coded CYC-B11, has been synthesized and demonstrated to be an efficient DSSC sensitizer [8]. This sensitizer, incorporating the electron-rich sulfur atom in between the alkyl substituent and bithiophene ring (Fig. 1A-Case IIB), provides the extension of π-conjugation to bipyridyl ancillary ligand, and improves the power conversion efficiency up to 11.5 %.

For the past two decades, the above mentioned heteroleptic Ru(II)-sensitizers molecular design has focused only on extending the π-conjugation of ancillary N3 ligands using alkyl-mono/bithiophene ligands and/or sulfur atoms, which improves the power conversion efficiency very little, i.e. from 10.0 to 11.5 %. This could be explained by the facts that such molecular design tends to attract most of the electrons from the Ru–NCS ligands to reside in the ancillary ligands (ineffective MLCT transitions), rather than to reside in that of anchoring ligands (effective MLCT transitions). This could limit the utilizations of the effective MLCT transitions for electrons injection into the TiO_2. Based on the simulated UV–visible absorption spectra of the C101 and C106 dye-sensitizers, we found that their UV absorption band (ineffective MLCT band, $\lambda < 400$ nm) intensities are increased significantly compared to that of N3 sensitizer; while their visible absorption band (effective

MLCT band, $\lambda \approx 530$ nm) are only slightly red-shifted (supplementary Fig S1). These phenomena, thus, indicate that the any structure modifications on the ancillary ligands of N3 dye increase the ineffective MLCT contributions.

Here using the density functional theory (DFT) and time dependent DFT (TD-DFT) methods, we develop a different strategy to selectively improve the effective MLCT contributions by modifying the molecular structure of the anchoring ligands (Fig. 1B). This modification is basically rationalized by (1) extending the π-conjugation of the anchoring ligands and (2) increasing their electron-acceptor abilities. We designed a novel anchoring ligand, namely 4,4′-di(2-carboxy-2-cyanovinyl)-2,2′-bypyridinyl (designated –CC ligand). This –CC anchoring ligand was then utilized to modify the molecular structure of the selected heteroleptic Ru-sensitizers, namely C101, C106, and CYC-B11, and to form their corresponding analogue-sensitizers, termed C101-1, C106-1, and CYC-B11-1, respectively (Fig. 1B). These analogue sensitizers were used as a model system to systematically demonstrate the unique properties of the designed anchoring ligand and to assess its contribution to the effective MLCT transition.

Computational details

All the calculations were carried out using the Gaussian 09 program package [15]. We employed the B3LYP exchange correlation functional [16, 17] combined with the standard double-ζ plus polarization basis set, 6-31G* [18, 19] to optimize the geometrical molecular structures of the selected heteroleptic C101, C106, and CYC-B11 Ru-dye sensitizers, together with their analogues. There is no artificial symmetric or geometric constraint was used during the optimization process. The ruthenium atom was described by using the LANL2DZ effective core potential function [20–22], where the central Ru ion was considered as Ru^{2+} with the electronic configuration of $4d^6$. Meanwhile for the description of other atoms (i.e. carbon, oxygen, nitrogen, sulfur, and hydrogen), the 6-31G* basis set was used. For the computation convenience in terms of saving time and resources, Na^+ in the experimental anchoring ligand of C101 and C106 complexes were replaced by H^+; similarly the $N(C_4H_9)_4^+$ in CYC-B11 complex was also replaced by H^+. Additionally, the long alkyl chain $N(C_4H_9)_4^+$ in the ancillary ligand of CYC-B11 complex was also replaced by H^+. These substitutions were checked not to lead to appreciable changes in their electronic properties.

TD-DFT method was used to calculate the energies and intensities of the 25 lowest-energy electronic transitions of all the Ru-sensitizers. These were transformed, using the SWizard program [23, 24], into simulated spectra as described before using Gaussian functions with half-widths of 3,000 cm^{-1}, as shown in following equation.

$$\varepsilon(\omega) = c_1 \sum_I \frac{f_I}{\Delta_{1/2,I}} \exp\left(-2.773 \frac{(\omega - \omega_1)^2}{\Delta_{1/2,I}^2}\right) \quad (1)$$

where ε is the molar extinction coefficient, given in units of M^{-1} cm^{-1}; the energy ω of all allowed transitions included in Eq. (1), is expressed in cm^{-1}; f_I and $\Delta_{1/2}$ are representing the oscillator strength and the half-bandwidths (3,000 cm^{-1}), respectively. All the parameters used in this equation are obtained using the combination of the BH and HLYP function [25, 26], which has been known to give the correct asymptotic behavior of the electronic transitions, with the 6-31+G* basis set [27].

Results and discussion

DFT is a promising approach to generate possible electronic-structures for large nanoscale systems, while TD-DFT offers a rigorous first-principles route to access the optical properties of large molecular systems containing hundreds of atoms [28]. A combination of the two approaches has been successful in determining ground-state geometries, vibrational spectra, and photoexcitation data related to many large molecules, including π-conjugated dye-sensitizers [2, 29–34]. The worth of the combined DFT and TD-DFT calculations in constructing the heteroleptic Ru(II)-sensitizers from the novel –CC anchoring ligand was verified by comparing the calculated results with those from reported experimental data.

Benchmark calculations

Figure 2 (inset) and Table 1 show the structural labeling scheme for N3 and the corresponding, experimental and calculated structural parameters, respectively. As shown in Fig. 2 (inset), the geometry of the N3 dye-sensitizer with a *cis* arrangement of the thiocyanate ligands results in an optimized pseudo octahedral *C*2 symmetry [11, 29, 31]. It can be seen from Table 1 that the calculated results are coincides with the available experimental values [35]. It is noteworthy that our optimized structural parameters are also consistent with previously reported DFT studies on this N3 dye-sensitizer [11, 29]. Also, the TD-DFT single point calculations have been performed for N3, C101, C106 and CYC-B11 dye sensitizers using BHandHLYP/6-31+G* level of theory, based on the optimized ground state geometries and the calculated absorption energy values are shown in Table S1 (Supplementary material). The simulated absorption spectrum of the above sensitizers was compared with the available experimental data. It is

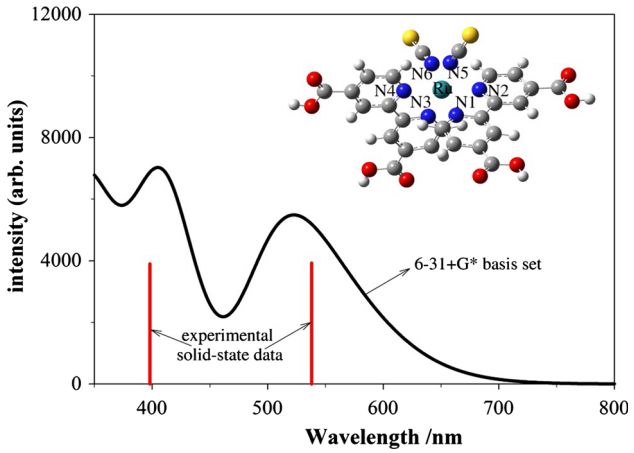

Fig. 2 Simulated UV–visible absorption spectrum of dye-sensitizer model N3, compared with the experimental solid-state data (*red vertical line*). *Inset* The optimized structure of the N3 dye-sensitizer

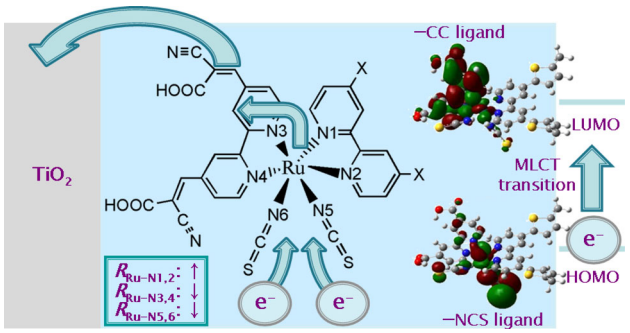

Scheme 1 Illustration of the effective metal-to-ligand charge transfer on Ru(II)-based dye sensitizers that incorporate the novel –CC anchoring ligand. Their corresponding frontier molecular orbitals at the HOMO and LUMO energy levels are also presented

Table 1 Optimized structural parameters [bond length in Å and angle in ° (degrees)] of model N3 dye-sensitizer compared with X-ray data and related DFT-calculation

Parameters	This work	Experimental[a]	Calculation[b]
$R_{Ru–N1,3}$	2.084	2.036	2.079
	2.084	2.058	2.079
$R_{Ru–N2,4}$	2.080	2.030	2.056
	2.080	2.013	2.056
$R_{Ru–N5,6}$	2.060	2.048	2.036
	2.060	2.046	2.036
$R_{N–C\ (NCS)}$	1.185	1.162	1.185
$R_{S–C\ (NCS)}$	1.627	1.615	1.628
∠N1–Ru–N2	78.6	79.8	78.9
∠N1–Ru–N3	93.7	90.6	95.1
∠N1–Ru–N4	99.9	97.8	94.0
∠N2–Ru–N4	177.9	174.5	169.5
∠N5–Ru–N6	92.3	NA	90.2

[a] Results taken from Ref. [35]. [b] Results taken from Ref. [11]. Except for the bond lengths of N–C and S–C of –NCS ligand, results are compared with references no. [29] (calculation) and no. [31] (experimental)

noteworthy that our computed UV–visible absorption bands agree with corresponding experimental values [8, 13, 36, 37]. Overall, these findings indicate the reliability of the present approach using DFT–TD-DFT calculations.

Designing the new Ru based sensitizer

Our molecular design aims to direct the HOMO–LUMO electronic transitions to preferentially follow the effective MLCT transition rather than the ineffective MLCT transition. To achieve this, the molecular structure of anchoring ligands of C101, C106, and CYC-B11 were altered, by inserting cyanovinyl-branches between the carboxyl (–COOH) groups and the bypyridine rings of the anchoring ligands (see Scheme 1). The cyanovinyl-branches are constructed using the C≡N group and C=C double bonds and the resulting anchoring ligand (termed a –CC ligand), then behaves as a primary "electron-acceptor" in the LUMO. The C≡N groups and C=C double bonds in the cyanovinyl-branches were selected for two reasons: first, the C≡N group is highly electronegative, i.e. 3.46, [38] thus electrons inhabiting the LUMO are attracted by the polarized nitrile residue's N atom [39, 40] and are finally delocalized in the whole –CC anchoring ligand. The higher electronegativity and subsequent delocalization in –CC anchoring ligand, makes this anchoring ligand as an effective "electron-acceptor". Previous studies show that the presence of the cyano (C≡N) group makes the anchoring group as key component in the LUMO [41, 42]. Also, The introduction of a C=C double bonds increase the π-conjugation, leading to electron-delocalization and a reduced the energy gap in the HOMO–LUMO transition [43–45]. It should be noted that our strategy is completely different to those previously reported [7, 8, 13, 14, 46–48] in the past two decades, which have only focused on altering the ancillary ligands. In those previous strategies, the resulting LUMO still comprised the anchoring and the ancillary ligands with nearly-equal electron density contributions.

Geometrical parameters of designed dyes

Fig S2 shows the representations of the optimized analogue dye-sensitizer structures together with their corresponding reference dye sensitizers. They were optimized using B3LYP/6-31G* level of theory. The calculated geometrical parameters are tabulated in Table 2. The optimized structure for each dye-sensitizer was found to be a Ru-centered

Table 2 Optimized structural parameters [bond length in Å and angle in °] for the analogue dye-sensitizers: C101-1, C106-1, and CYC-B11-1, in comparison with their corresponding reference dye-sensitizers: C101, C106, and CYC-B11

Parameters	C101-1	C101	C106-1	C106	CYC-B11-1	CYC-B11
$R_{Ru–N1,2}$	2.104	2.097	2.104	2.094	2.104	2.096
	2.094	2.091	2.094	2.091	2.094	2.090
$R_{Ru–N3,4}$	2.058	2.072	2.059	2.074	2.058	2.073
	2.069	2.074	2.067	2.074	2.069	2.074
$R_{Ru–N5,6}$	2.061	2.067	2.063	2.069	2.061	2.068
	2.053	2.061	2.051	2.059	2.051	2.060
$R_{N–C\ (NCS)}$	1.186	1.185	1.186	1.186	1.186	1.185
$R_{S–C\ (NCS)}$	1.627	1.630	1.628	1.630	1.627	1.630
∠N1–Ru–N2	77.7	77.9	77.7	77.9	77.7	77.9
∠N1–Ru–N3	94.1	94.1	94.0	94.5	94.0	94.4
∠N1–Ru–N4	100.9	100.6	100.9	100.5	100.7	100.7
∠N1–Ru–N6	172.2	172.2	172.1	172.2	177.2	172.3
∠N2–Ru–N4	177.7	177.7	177.5	177.9	177.4	177.8
∠N5–Ru–N6	92.7	93.1	92.9	93.1	92.8	93.1

complex, in which the Ru ion is present as Ru^{2+} with a $4d^6$ electronic configuration. The dicarboxy-bipyridine anchoring ligands are planar, while the two non-attached bithiophene ancillary ligands bend slightly downward. These sensitizers show almost symmetric arrangement of the ligands; however, the octahedral disposition of the N atoms around the Ru-center is slightly distorted due to the different nature of these ligands, as evidenced by the calculated angles of the N1–Ru–N3 and N1–Ru–N6 being slightly different from the ideal values of 90.0° and 180.0° for an octahedral complex (see Table 2). Importantly, for the C101-1, C106-1, and CYC-B11-1 dye-sensitizers, the bond lengths of Ru–N i.e. to the "electron-donor" –NCS ($R_{Ru–N5}$ and $R_{Ru–N6}$) and to the "electron-acceptor" –CC anchoring ($R_{Ru–N3}$ and $R_{Ru–N4}$) ligands, were found to be slightly shorter than the corresponding bond lengths in the reference dye-sensitizers (see Table 2). It is noteworthy that the interactions Ru–N3,4 (Ru–CC) and Ru–N5,6 (Ru–NCS) are the key parameters for the effective MLCT transition, lead to contraction of the bond lengths. This may due to a strong electron-coupling between the electron-donating –NCS ligand and the electron-accepting –CC anchoring ligand through the Ru-bridge. In contrast, the bond lengths of Ru–N1 and Ru–N2, from the thiophene-functionalized ancillary ligands, become longer. Overall, our findings on the longer bond lengths of $R_{Ru\text{-}N1,2,}$ and shorter bond lengths of $R_{Ru–N3,4}$ and $R_{Ru–N5,6}$, emphasize that the effective MLCT transition is more favored than the ineffective one.

Absorption spectra

Having verified the DFT–TD-DFT calculations using the N3 dye-sensitizer model, similar calculations were then used to construct molecular structures for the selected heteroleptic sensitizers, i.e. C101, C106, and CYC-B11, as well as their analogue sensitizers, i.e. C101-1, C106-1, and CYC-B11-1, respectively. To highlight the viability of the present strategy, especially the role of the –CC anchoring ligand as the efficient "electron-acceptor" able to enhance the effective MLCT transitions, the UV–visible absorption spectra of the developed dye-sensitizers were simulated and compared with the corresponding absorption spectra of the reference-sensitizers. The UV–visible spectra for the developed analogue-sensitizers and their corresponding reference-sensitizers were simulated using BHandHLYP/6-31+G* level of theory and shown in Fig. 3. As can be seen from this fig, the absorption spectra in both the UV and visible regions, for the analogue-sensitizers, i.e. C101-1, C106-1, and CYC-B11-1, are red-shifted compared to their reference-sensitizers. It has been found that, all the developed analogue-sensitizers showed red shifts of about 30–65 nm and significant increases in intensity also noted in their visible region absorption spectra, depending on their reference-sensitizers. This finding is significant because the most of the effective MLCT transitions occur in this region. In addition to this visible-absorption peak, a unique shoulder peak, assigned to the effective MLCT transitions, located in the near IR region, was generated by the insertion of the cyanovinyl-branches within a –CC anchoring ligand, as indicated by the enclosed black ring.

Apart from the visible-to-near IR absorption region, it is noteworthy that the UV absorption spectra for all the developed analogue-sensitizers were red-shifted by about 40 nm, compared to their reference sensitizers (Fig. 3). It is also evident that the UV absorption spectra for all reference sensitizers (i.e. C101, C106, and CYC-B11) are similarly centered at a wavelength ~360 nm, proving that previous

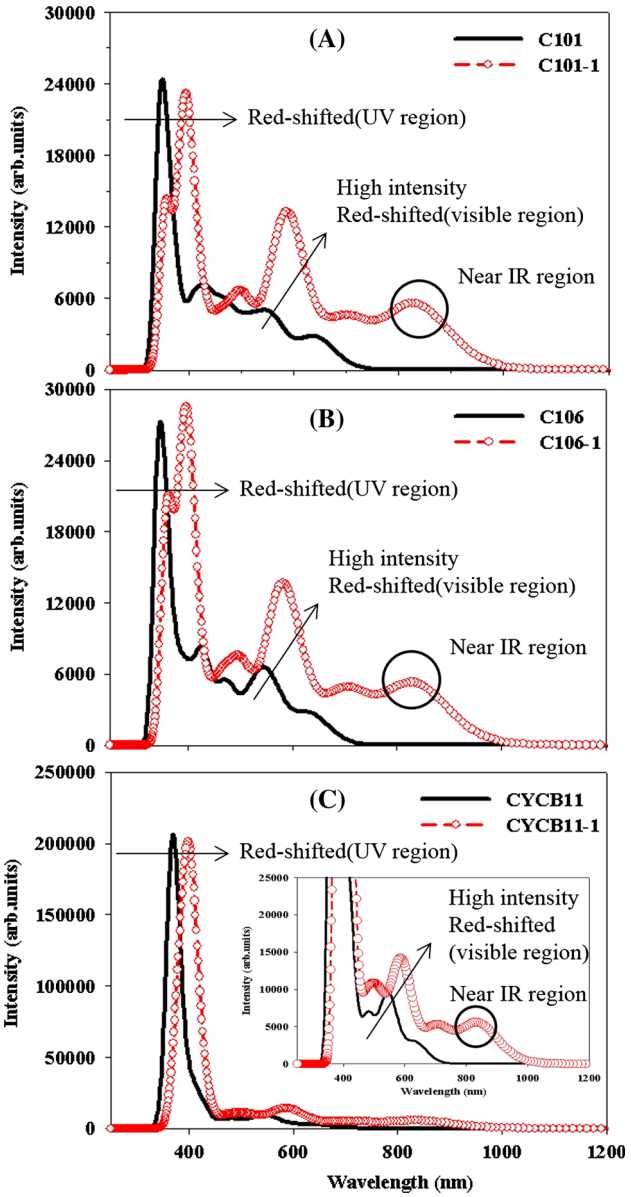

Fig. 3 Simulated UV–visible absorption spectra of the developed dye-sensitizers: **A** C101-1, **B** C106-1, and **C** CYC-B11-1, in comparison with their corresponding reference dye-sensitizers: C101, C106, CYC-B11-1, respectively. For the inset figure of panel (**C**), the scale of its ordinate (i.e. intensity) is also presented using a same scale with those of panels **A**, **B**

strategies with modified N3 sensitizer ancillary ligands are unable to red-shift the absorption spectra in the UV region. In contrast, our strategy utilizing cyanovinyl-branches inserted in the –CC anchoring ligand, is able to red-shift the absorption spectra in the UV region. It is believed that this phenomenon may reflect the transformation of an ineffective transition into an effective MLCT transition. Thus, a simultaneous red shift in both the UV–visible absorption spectra accompanied by an increase in visible absorption intensity may be indicative of an environment conducive to the enhancement of MLCT transitions.

Electronic structure

It is well-known that molecular orbital (MO) contributions are of great importance in determining the optical properties of Ru(II) dye-sensitizers. Here a small HOMO–LUMO gap is prerequisite, since it is crucial in determining the efficiency of the effective MLCT contributions. To improve these effective MLCT contributions, the HOMOs should be localized on the donor subunit (e.g. –NCS ligand) and the LUMOs on the acceptor subunit (e.g. anchoring ligand). Table 3 lists the transition wavelengths, oscillator strengths, and transition assignments for the most relevant HOMO-to-LUMO optical transitions of the UV–visible spectra shown in Fig. 3. As we mentioned earlier, a HOMO–LUMO transition that commences from an "electron-donor" –NCS ligand to an "electron-acceptor" –CC ligand, will be classified as an effective MLCT transition; other transitions, e.g. from the –NCS ligand to the ancillary ligand, will be classified as ineffective.

The isodensity plots of the frontier MOs for all dye-sensitizers were built using B3LYP/6-31G* level of theory. Figure 4 shows these isodensity plots for the developed C101-1 sensitizer and its reference sensitizer C101; this representative pair of sensitizers will be used for our discussion. The isodensity plots for the other dye-sensitizers, that is, C106, C106-1, CYC-B11, and CYC-B11-1, are given in the Fig S3 of supplementary material. It is clear that from Figs. 4 and S3, that the patterns of the HOMOs for all the developed sensitizers are qualitatively similar. For the C101-1 sensitizer (Fig. 4B), its three highest HOMOs, i.e. HOMO to HOMO-2 have essentially a ruthenium t_{2g} character with a sizable contribution coming from the –NCS ligand orbitals. This results from the nonbonding combinations of the Ru $t2g$ orbitals (d_{xy}, d_{xy}, and d_{yz}) with the π-orbitals of –NCS ligands. The LUMOs for this developed sensitizer are found to be a set of –CC anchoring ligand orbitals, excluding LUMO + 2 and LUMO + 4. Overall, the LUMOs are essentially localized over the whole –CC anchoring ligand unit, with the maximum electron density being associated with its pyridine-rings, cyanovinyl-branches, and carboxyl groups. This highlights the fact that the cyanovinyl-functionalized –CC anchoring ligands have a good ability as an "electron-acceptor". In DSSCs, such orbital contributions with the stabilization of π* orbitals localized on these –CC anchoring ligands should favour electron injection from the dye-sensitizer to the CB of the semiconductor's surface. It should be noted that the patterns of the HOMOs and LUMOs for the other developed sensitizers, i.e. the C106-1 and CYC-B11-1, follow a similar tendency to C101-1.

Table 3 The most representative excitation wavelength, oscillator strengths, and dominant excitation character of the developed analogue dye-sensitizers: C101-1, C106-1, and CYC-B11-1 in comparison with their corresponding reference dye-sensitizers: C101, C106, and CYC-B11, respectively

Dye-sensitizers	Transition wavelength (λ, nm)	State	Oscillator strength (f)	Transition assignment
C101-1	833.2	S0 → S1	0.050	H → L (72 %)*, H-2 → L (9 %)*
	589.9	S0 → S5	0.097	H-2 → L (55 %)*, H → L+1 (19 %)*,
	390.9	S0 → S17	0.142	H-2 → L+1 (9 %)*, H → L (8 %)*
				H-6 → L (34)**, H-5 → L (25 %)**, H-2 → L+3 (12 %)*
C101	561.2	S0 → S2	0.033	H-1 → L (72 %)*, H-2 → L (15 %)*, H → L (5 %)*
	511.9	S0 → S4	0.030	
	344.7	S0 → S24	0.142	H → L+1 (86 %)**
				H-1 → L+5 (37 %)**, H-2 → L+5 (27 %)**,
				H-3 → L+3 (15 %)**, H-2 → L+3 (7 %)**
C106-1	834.5	S0 → S1	0.047	H → L (74 %)*, H-2 → L (7 %)*
	585.1	S0 → S5	0.095	H-3 → L (61 %)*, H → L+1 (17 %)*,
	392.6	S0 → S17	0.163	H-3 → L+1 (8 %)*, H → L (6 %)*
				H-6 → L (25)**, H-2 → L+3(14 %)*,
				H-5 → L (13)**, H-7 → L (13 %)**,
				H-1 → L+3 (9 %)*, H-8 → L (7 %)**,
				H → L+4 (5 %)**
C106	559.6	S0 → S2	0.039	H-1 → L (83 %)*, H → L (5 %)*
	526.0	S0 → S4	0.029	H → L+1 (63 %)**, H-2 → L (18 %)*,
	340.3	S0 → S25	0.129	H-1 → L (6 %)*
				H-6 → L (16 %)**, H-1 → L+3 (15 %)**,
				H-5 → L (6 %)**, H-3 → L+3 (6 %)**,
				H-1 → L+5 (5 %)*
CYC-B11-1	840.3	S0 → S1	0.049	H → L (73 %)*, H-2 → L (8 %)*
	591.3	S0 → S5	0.099	H-3 → L (58 %)*, H → L+1 (19 %)*,
	390.9	S0 → S20	0.142	H-3 → L+1 (8 %)*, H → L (7 %)*
				H-5 → L+2 (25 %)**, H-5 → L (17 %)**,
				H-6 → L (11 %)*, H → L+3 (7 %)*,
				H-5 → L+3 (5)*
CYC-B11	560.1	S0 → S2	0.046	H-1 → L (74 %)*, H-2 → L (7 %)*,
	535.1	S0 → S3	0.024	H → L (6 %)*
	369.0	S0 → S19	0.137	H → L+1 (47 %)**, H-2 → L (31 %)*,
				H-2 → L+1 (6 %)*
				H-1 → L+2 (27 %)**, H-2 → L+2 (15 %)**,
				H-7 → L (14 %)**, H-1 → L+4 (8 %)**

* Effective MLCT transitions

** Ineffective MLCT transitions

With the aid of the isodensity plots of the frontier MOs, all the effective MLCT transitions presented in Table 3, can be easily identified. In our example, the broad absorption band in the visible region (ca. 520.8 nm) for the C101 reference sensitizer, appears to be mainly composed of two strong transitions, namely the effective MLCT transition located at 561.2 nm, and the ineffective transition at 511.9 nm (Table 3). Among these two transitions, the effective MLCT transition originates from the transitions H-1 → L (72 %), H-2 → L (15 %), and H → L (5 %). and ineffective transition originates from the H → L+1 (86 %) and corresponds to an electron transfer from the mixed Ru t_{2g} and NCS π orbitals to the unoccupied π* orbital of the alkyl-bithiophene-functionalized ancillary ligands (see Table 3; Fig. 4A). This ineffective transition also competes with that of effective MLCT transition, and consequently limits the C101 sensitizer's ability to inject an electron from the anchoring ligand to the semiconductor's surface. It is noteworthy that this competition effect is highly suppressed in the case of the C101-1 sensitizer, as its absorption band (see Fig. 3), particularly in the visible region (ca. 584.8 nm; 64 nm red shifted compared with that of C101 reference), appears to be mainly an effective MLCT transition. This effective MLCT

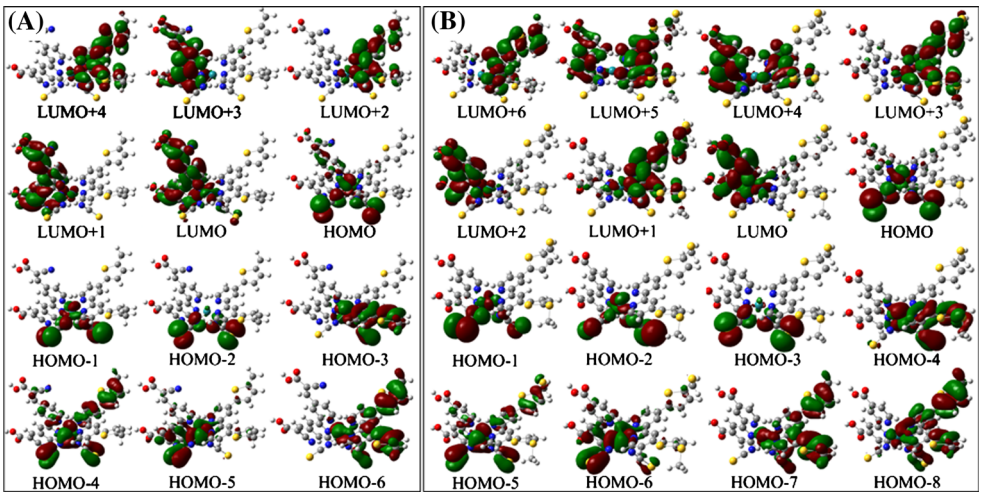

Fig. 4 Frontier molecular orbitals of **A** the developed C101-1 dye-sensitizer, calculated at B3LYP/6-31G* level of theory. They were compared with that of **B** reference C101 dye-sensitizer. All the isodensity surface values are fixed at 0.02

transition is basically originates from a series of transitions in the range 502.4–620.5 nm. Among the spaced peaks, the strongest intensity appears at 589.9 nm (much higher than that of C101 reference), and involves mixed transitions of H-2 → L (55 %), H → L+1 (19 %), H-2 → L+1 (9 %), and H → L (8 %). It should be noted here that the present strategy, i.e. by the insertion of the cyanovinyl-branches inside the –CC anchoring ligand of the developed C101-1 sensitizer, gives this sensitizer a wider and stronger absorption band in the visible region, which is in-line with the requirements for a high performance dye-sensitizer.

In addition to this visible-absorption band, the present strategy also generates a shoulder peak that is located in the near-IR region, centered at 775.2 nm, as shown in Fig. 3. As can be seen from Table 3, this absorption band is associated with the transitions H → L (72 %) and H-2 → L (9 %), and belongs to the effective MLCT transition. Both the absorption bands the transitions H → L (72 %) and H-2 → L (9 %), and belongs to the effective MLCT transition. Both the absorption bands in the visible-to-near IR region, for the developed C101-1 sensitizer, contains mixed transitions from the Ru–NCS of HOMOs to the –CC anchoring ligands of LUMOs, thus greatly enhancing the ability of the effective MLCT transition to improve electron injection efficiency. Returning to the reference C101 sensitizer, the observed strong absorption band in the UV region located at 352 nm (Fig. 3) results largely from ineffective transitions. Specifically, from the strongest contribution ($f = 0.142$ and $\lambda = 344.7$ nm; Table 3), these ineffective transitions originate from the transitions of H-1 → L+5 (37 %), H-2 → L+5 (27 %), H-3 → L+3 (15 %), and H-2 → L+3 (7 %). These transitions correspond to electron transfers mostly from the mixed Ru t_{2g} and NCS π orbitals to the unoccupied π* orbital of the alkyl-bithiophene-functionalized ancillary ligands (see Table 3; Fig. 4A). It is noteworthy that using the present strategy, these ineffective transitions can be partially transformed into effective MLCT transitions, as evidenced by the presence of the effective MLCT transition, i.e. H-2 → L+3 (12 %), among the other electronic transitions at 390.9 nm ($f = 0.142$) for the C101-1 sensitizer (see Table 3). Consequently, the absorption band for this C101-1 sensitizer is red-shifted, by about 40 nm, compared to its reference C101 sensitizer. To the best of our knowledge, this unique finding is essential for the DSSCs' applications, since most of the reported strategies are as yet unable to red-shift the UV absorption spectrum. Through this finding, we conclude that by red-shifting the UV absorption spectrum to the near-visible region, i.e. higher than 400 nm, the ineffective transitions can be partially altered into effective MLCT transitions. It should also be noted that the observed electronic transitions within the UV–visible absorption spectra for other developed sensitizers, i.e. C106-1 and CYC-B11-1, follow a similar tendency with that of previously discussed C101-1 sensitizer, thereby suggesting our strategy can be generally applied to other dye-sensitizers.

Density of states (DOS)

Figure 5 shows the relationship between the energy gap of the HOMO-to-LUMO transition and the DOS pattern, for both of the developed and reference dye-sensitizers. Taking the C101 reference sensitizer (Fig. 5A) as an example, its HOMO–LUMO gap value is 1.64 eV, while its DOS pattern, particular in the first oscillation, shows that the HOMOs states are composed of mixed Ru-metal and "electron-donor" –NCS ligands, with the major contribution coming from the –NCS ligands. More specifically, the degree of localization of electrons in the –NCS ligands is found to be 81 %, compared to 14 % for Ru-metal (see Fig. 6A). Meanwhile, the LUMOs states' DOS pattern at

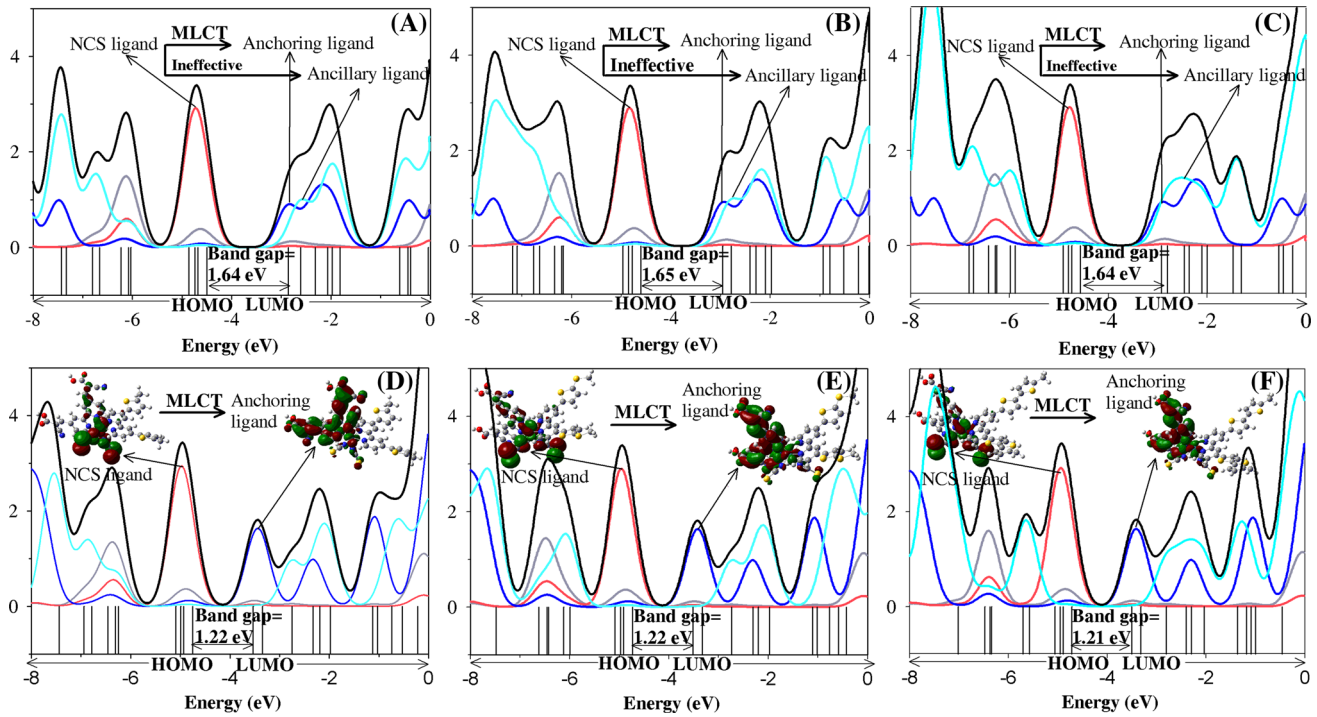

Fig. 5 Relationship between the energy gaps of HOMOs-to-LUMOs transitions with the density of states, of the reference dye-sensitizers: **A** C101, **B** C106, and **C** CYC-B11. They were compared with that of the developed dye-sensitizers: **D** C101-1, **E** C106-1, and **F** CYC-B11-1, respectively. *Inset* The frontier MOs of HOMO–LUMO

for this sensitizer comprises two different ligands, namely the anchoring- and the ancillary-ligands; both of which have a similar composition, more precisely: 58 % of the electrons are localized in the anchoring ligands, and 33 % are localized in the ancillary ligands. Overall, these findings illustrate that electronic transitions concerning HOMOs to LUMOs states are contributed-to by two different transition directions: the first, where the electrons are transferred from the –NCS ligand to the anchoring ligands, which are akin to effective MLCT transitions; and the second, where the electrons are transferred from the –NCS ligand to the anchoring ligands, these being akin to ineffective transitions. These competition effects, which have been discussed in relation to the electronic-transitions shown in Table 3, limit the effectiveness of the C101 sensitizer by hindering electron injection from the anchoring ligand to the semiconductor's surface. It is interesting to note that after employing the present strategy, via the insertion of cyanovinyl-branches into the anchoring ligand, the HOMO–LUMO energy gap for the developed C101-1 sensitizer decreased to 1.2 eV (see Fig. 5D). The energy gap decrease ($\sim$0.42 eV), dramatically alters the configuration of the MOs: e.g. the LUMO states, with 89 % of electron density, of this sensitizer were found to mainly originate from the "electron-acceptor" –CC anchoring ligands (see Fig. 6D). This together with the findings related to the HOMOs states, which mainly arise from the NCS ligands (81 %), strongly emphasizes the fact that most of the electronic-transitions in this sensitizer are effective MLCT transitions that suppress competition from the C101 sensitizer. As can be seen from Fig. 5A–D, the HOMO of all the developed sensitizers almost remains its original position, whereas the LUMO levels are decreased significantly after the inclusion of the cyanovinyl-branches into the anchoring ligand. This confirms the earlier studies [43–45, 49] that presence of the electron withdrawing cyanovinyl group has the potential of lowering the LUMO level, which leads to redshift the absorption spectra of the designed sensitizers. It is noteworthy that the other developed sensitizers, i.e. C106-1 and CYC-B11-1, have a similar behavior with that of previously demonstrated C101-1 sensitizer, as these two developed sensitizers showed a good ability to lower their HOMO–LUMO energy gap, by about 0.43 eV (see Fig. 5E, F, respectively); importantly, these sensitizers are also able to alter most of the ineffective contributions into the effective MLCT contributions (Fig. 6E, F, respectively). From the above results, we found that the inclusion of cyanovinyl-branches into the anchoring ligand prominently increases the effective MLCT transition which resulted in significant red-shift of absorption spectrum in the Ru based designed sensitizers. However, further studies are necessary to

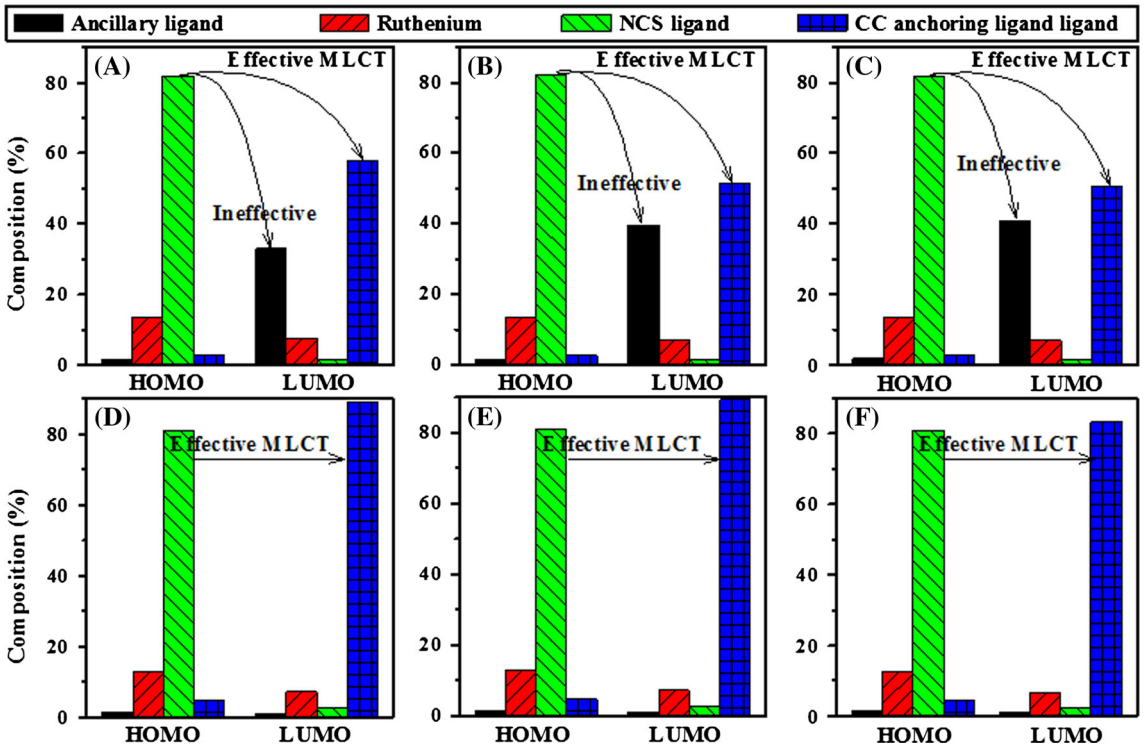

Fig. 6 The HOMOs–LUMOs composition of the reference **A** C101, **B** C106, and **C** CYC-B11 dye sensitizers. They were compared with that of the developed dye-sensitizers: **D** C101-1, **E** C106-1, and **F** CYC-B11-1, respectively. The composition values were obtained via a deconvolution of DOS curves of the Fig. 5

rationalize the efficiency of this new designed sensitizers towards the DSSC applications.

Conclusions

Quantum chemical calculations (DFT and TD-DFT) were used to design a novel ruthenium dye sensitizers by inserting the cyanovinyl-branches inside the anchoring ligands of selected highly efficient dye-sensitizers, namely C101, C106, and CYC-B11. Our calculated results show that the presence of cyanovinyl-branches within the backbone of –CC anchoring ligands of Ru(II)-sensitizers, gives rise to a red-shift in the UV–visible absorption spectra, simultaneously with an increase in the visible absorption intensity compared to the selected reference dyes. Also, we found that the present strategy not only red shift the absorption spectra, but change the ineffective MLCT transitions to the effective transition in the UV-visible region, which is required for the DSSCs' applications. We have shown that the presence of cyanovinyl-branches, have a strong electron-accepting ability which enhance the electron transfer from the "electron-donor" NCS ligand to the "electron-acceptor" –CC ligand. Also, this cyanovinyl-branches improves the contribution of LUMOs of anchoring group, which is more important in the electron injection from the dye to the conduction band of the semiconductor surface. The present calculated results clearly demonstrated that, the designed ruthenium dyes provide good performances as sensitizers compared to the selected efficient reference dyes and this study may provide the design strategy of the ruthenium dyes to achieve the best efficiency of DSSCs.

Acknowledgments We thank the National Science Council of Taiwan (NSC-98-2113-M011-001-MY3) for supporting this research financially and National Center of High-Performance Computing for computer time and facilities.

References

1. Hagfeldt A, Boschloo G, Sun LC, Kloo L, Pettersson H (2010) Chem Rev (Washington, DC) 110(11):6595–6663
2. Santhanamoorthi N, Lo CM, Jiang JC (2013) J Phys Chem Lett 4(3):524–530
3. Santhanamoorthi N, Lai KH, Taufany F, Jiang JC (2013) J Power Sour 242:464–471
4. Meyer GJ (2010) ACS Nano 4(8):4337–4343
5. Vougioukalakis GC, Philippopoulos AI, Stergiopoulos T, Falaras P (2011) Coord Chem Rev 255(21–22):2602–2621
6. Nazeeruddin MK, Kay A, Rodicio I, Humphry-Baker R, Mueller E, Liska P, Vlachopoulos N, Graetzel M (1993) J Am Chem Soc 115(14):6382–6390
7. Chen CY, Wu SJ, Wu CG, Chen JG, Ho KC (2006) Angew Chem-Int Ed 45(35):5822–5825

8. Chen CY, Wang MK, Li JY, Pootrakulchote N, Alibabaei L, Ngoc-le CH, Decoppet JD, Tsai JH, Gratzel C, Wu CG, Zakeeruddin SM, Gratzel M (2009) ACS Nano 3(10):3103–3109
9. Kuang DB, Ito S, Wenger B, Klein C, Moser JE, Humphry-Baker R, Zakeeruddin SM, Gratzel M (2006) J Am Chem Soc 128(12):4146–4154
10. Chen KS, Liu WH, Wang YH, Lai CH, Chou PT, Lee GH, Chen K, Chen HY, Chi Y, Tung FC (2007) Adv Funct Mater 17(15): 2964–2974
11. Fantacci S, De Angelis F, Selloni A (2003) J Am Chem Soc 125(14):4381–4387
12. Nazeeruddin MK, De Angelis F, Fantacci S, Selloni A, Viscardi G, Liska P, Ito S, Bessho T, Gratzel M (2005) J Am Chem Soc 127(48):16835–16847
13. Gao F, Wang Y, Shi D, Zhang J, Wang MK, Jing XY, Humphry-Baker R, Wang P, Zakeeruddin SM, Gratzel M (2008) J Am Chem Soc 130(32):10720–10728
14. Cao YM, Bai Y, Yu QJ, Cheng YM, Liu S, Shi D, Gao FF, Wang P (2009) J Phys Chem C 113(15):6290–6297
15. Frisch MJ, Trucks GW, Schlegel HB, Scuseria GE, Robb MA, Cheeseman JR, Scalmani G, Barone V, Mennucci B, Petersson GA, Nakatsuji H, Caricato M, Li X, Hratchian HP, Izmaylov AF, Bloino J, Zheng G, Sonnenberg JL, Hada M, Ehara M, Toyota K, Fukuda R, Hasegawa J, Ishida M, Nakajima T, Honda Y, Kitao O, Nakai H, Vreven T, Montgomery JA, Jr.;, Peralta JE, Ogliaro F, Bearpark M, Heyd JJ, Brothers E, Kudin KN, Staroverov VN, Kobayashi R, Normand J, Raghavachari K, Rendell A, Burant JC, Iyengar SS, Tomasi J, Cossi M, Rega N, Millam NJ, Klene M, Knox JE, Cross JB, Bakken V, Adamo C, Jaramillo J, Gomperts R, Stratmann RE, Yazyev O, Austin AJ, Cammi R, Pomelli C, Ochterski JW, Martin RL, Morokuma K, Zakrzewski VG, Voth GA, Salvador P, Dannenberg JJ, Dapprich S, Daniels AD, Farkas O, Foresman JB, Ortiz JV, Cioslowski J, Fox DJ (2009) Gaussian 09, Revision A.1 Wallingford: Gaussian, Inc
16. Becke AD (1993) J Chem Phys 98:5648–5652
17. Lee C, Yang W, Parr RG (1988) Phys Rev B 37(2):785–789
18. Rassolov VA, Ratner MA, Pople JA, Redfern PC, Curtiss LA (2001) J Comput Chem 22(9):976–984
19. Rassolov VA, Pople JA, Ratner MA, Windus TL (1998) J Chem Phys 109(4):1223–1229
20. Hay PJ, Wadt WR (1985) J Chem Phys 82(1):270–283
21. Wadt WR, Hay PJ (1985) J Chem Phys 82(1):284–298
22. Hay PJ, Wadt WR (1985) J Chem Phys 82(1):299–310
23. Gorelsky SI (2013) SWizard program. University of Ottawa, Ottawa. http://www.sg-chem.net/
24. Gorelsky SI, Lever ABP (2001) J Organomet Chem 635(1–2): 187–196
25. Becke AD (1993) J Chem Phys 98(2):1372–1377
26. Ditchfield R, Hehre WJ, Pople JA (1971) J Chem Phys 54(2): 724–728
27. Francl MM, Pietro WJ, Hehre WJ, Binkley JS, Gordon MS, DeFrees DJ, Pople JA (1982) J Chem Phys 77(7):3654–3665
28. Koch W, Holthausen MC (2000) A chemist's guide to density functional theory, 2nd edn. Willey-VCH, Weinheim
29. Guo P, Ma RM, Guo LS, Yang LL, Liu JF, Zhang XX, Pan X, Dai SY (2010) J Mol Graphics Model 29(3):498–505
30. De Angelis F, Fantacci S, Selloni A, Nazeeruddin MK (2005) Chem Phys Lett 415(1–3):115–120
31. De Angelis F, Fantacci S, Selloni A (2004) Chem Phys Lett 389(1–3):204–208
32. Le Bahers T, Labat F, Pauporte T, Laine PP, Ciofini I (2011) J Am Chem Soc 133(20):8005–8013
33. Monari A, Assfeld X, Beley M, Gros PC (2011) J Phys Chem A 115(15):3596–3603
34. Jacquemin D, Perpete EA, Scuseria GE, Ciofini I, Adamo C (2008) J Chem Theory Comput 4(1):123–135
35. Shklover V, Ovchinnikov YE, Braginsky LS, Zakeeruddin SM, Gratzel M (1998) Chem Mater 10(9):2533–2541
36. Shklover V, Nazeeruddin MK, Zakeeruddin SM, Barbe C, Kay A, Haibach T, Steurer W, Hermann R, Nissen HU, Gratzel M (1997) Chem Mater 9(2):430–439
37. Nazeeruddin MK, Zakeeruddin SM, Humphry-Baker R, Jirousek M, Liska P, Vlachopoulos N, Shklover V, Fischer CH, Gratzel M (1999) Inorg Chem 38(26):6298–6305
38. Mullay J (1985) J Am Chem Soc 107:7271–7275
39. Bratsch SG (1985) J Chem Educ 62(2):101
40. Boyd RJ, Edgecombe KE (1988) J Am Chem Soc 110:4183–4186
41. Katono M, Bessho T, Meng S, Humphry-Baker R, Rothenberger G, Zakeeruddin SM, Kaxiras E, Gratzel M (2011) Langmuir 27(23):14248–14252
42. Ho HA, Brisset H, Frere P, Roncali J (1995) J Chem Soc Chem Commun 22:2309–2310
43. Hara K, Sayama K, Ohga Y, Shinpo A, Suga S, Arakawa H (2001) Chem Commun (Cambridge, UK) (6):569–570
44. Hara K, Tachibana Y, Ohga Y, Shinpo A, Suga S, Sayama K, Sugihara H, Arakawa H (2003) Sol Energy Mater Sol Cells 77(1):89–103
45. Sayama K, Tsukagoshi S, Mori T, Hara K, Ohga Y, Shinpou A, Abe Y, Suga S, Arakawa H (2003) Sol Energy Mater Sol Cells 80(1):47–71
46. Chen CY, Wu SJ, Li JY, Wu CG, Chen JG, Ho KC (2007) Adv Mater (Weinheim, Ger.) 19(22):3888–3891
47. Gao FF, Wang Y, Zhang J, Shi D, Wang MK, Humphry-Baker R, Wang P, Zakeeruddin SM, Gratzel M (2008) Chem Commun (Cambridge, UK) (23):2635–2637
48. Yu QJ, Liu S, Zhang M, Cai N, Wang Y, Wang P (2009) J Phys Chem C 113(32):14559–14566
49. Huang ST, Hsu YC, Yen YS, Chou HH, Lin JT, Chang CW, Hsu CP, Tsai C, Yin DJ (2008) J Phys Chem C 112(49):19739–19747